EFFECTS OF DYNAMIC SEGREGATION AND ENVIRONMENT ON CRACK GROWTH AT ELEVATED TEMPERATURE

P. Bowen*, C.A. Hippsley** and J.F. Knott*

The paper describes work carried out to examine mechanisms of subcritical growth in quenched 2¼Cr-1Mo steel at 500 °C, in air and in vacuum. For static stress intensities of less than 55 MPa √m in vacuum, the mode of fracture is smooth low ductility intergranular fracture (LDIGF), produced by the dynamic segregation of sulphur to the crack tip. In air, interaction with the environment enhances crack growth dramatically. Intergranular cracking can also occur during fatigue in air and in vacuum. Large increases in crack increment per cycle are observed as the frequency is reduced and these can be predicted from base-line fatigue data and static crack growth resistance curves.

INTRODUCTION

The problems associated with the stress relief cracking of thick-section welded joints have long been recognised in the pressure-vessel industry. The stress-relieving heat treatment is necessary both to improve weld metal toughness, and to reduce the residual stresses present after welding. It is performed typically at temperatures in excess of 600 °C. However, during such post-weld heat-treatment, cracking may occur exclusively along prior austenite grain boundaries particularly in coarse grained heat affected zone regions. Such cracking could produce an extended defect which might threaten the structural integrety of the component or vessel during its design life, and illustrates the need to perform non-destructive testing validations after any post-weld heat treatments. Although the engineering significance of stress-relief cracking or reheat cracking, may often be reduced through modified welding practise or compositional control, the underlying mechanism of crack growth is of considerable scientific interest. Under static loading conditions two distinct forms of intergranular cracking have been observed: (1) smooth, low ductility inter-

* Department of Metallurgy and Materials Science, Cambridge University
** Atomic Energy Research Establishment, Harwell, Oxon.

granular cracking (LDIGF) and typically occurring at temperatures of 300-600 °C, (ii) intergranular microvoid coalescence (IMVC), typically occurring at temperatures of 500 - 700 °C. Intriguingly, subsequent fracture at low temperatures (e.g. -196 °C) of a testpiece unloaded from a temperature in the range 300 to 700 °C does not produce any intergranular fracture. It is clear, therefore, that the mechanism of subcritical intergranular cracking occurs only under the conjoint action of stress and temperature and is a dynamic mechanism of crack growth.

If this mechanism can also occur under fatigue loading, then it would be expected to affect fatigue crack growth rates. Such a system could then be of great potential use for the study of monotonic/cyclic interactions, which might serve as a general model for crack growth in creep/fatigue conditions. Significant advances in understanding the fundamental mechanism of crack growth under static loading have recently been made, particularly by using high resolution Scanning Auger Microscopy. Sulphur has been identified as the primary embrittling species. Current micro-mechanistic models threat the dynamic segregation of sulphur under stress to regions in close proximity to the tips of sharp cracks (Hippsley et al. (1), Shin and McMahon (2)).

The present paper reports a number of recent studies performed to examine high-temperature fracture in quenched 2¼Cr-1Mo pressure vessel steel under both monotonic and cyclic loading, in air and in vacuum, at the single test temperature of 500 °C. Carefully controlled heat treatments have been performed in order to address the mechanisms of cracking in well characterised uniform (martensitic) microstructures. In particular, attention has been paid to the influence of sulphur (present either in solid solution, or as manganese sulphides) on the susceptibility of a material to cracking.

EXPERIMENTAL

All tests were carried out on a commercial grade of 2¼Cr-1Mo steel plate whose composition is given in table 1. Notched bend testpieces of the geometry shown in figure 1 were machined in the transverse short transverse (TST) orientation, and heat treated individually in a vacuum furnace with temperature control to ± 5 °C. The heat treatment schedules are shown in figure 2, and all initially involve austenitising at 1300 °C for 30 minutes, followed by either direct water quenching, or furnace cooling to lower austenitising temperatures of 1200, 1100, 1000 and 900 °C respectively, held for 1 hr, and followed by water quenching (step quenching). This schedule results in a constant prior austenite grain size of approximately 200 μm and similar strength levels for all testpieces. Table 2 shows the hardness and proof stress values obtained from testpieces subjected to the extremes of heat treatments employed.

Such heat treatments have been shown to produce uniform martensitic microstructures with different concentrations of phosphorus at prior austenite grain boundaries: note that step quenching increases the amount of phosphorus at such boundaries, thereby promoting intergranular decohesion and reducing values of fracture toughness measured at low temperatures (Bowen et al. (3)). These heat treatments are also predicted to vary the amount of sulphur remaining in solid solution, see table 3 following Turdogan et al. (4), and have recently also been observed to affect the distribution of manganese sulphides (Hippsley et al. (5)).

All mechanical tests were performed using servo-hydraulic testing machines, equipped with vacuum chambers and quartz lamp heating facilities. The tests were run under interactive computer control. The test temperature was maintained at 500 ± 2 °C.

Static tests were conducted at atmospheric pressure, at approximately $\leq 1.10^{-3}$ mbar total pressure, and at approximately 2.10^{-7} mbar total pressure (as measured by a mass spectrometer). In all cases, fatigue pre-cracks were grown to a distance of 0.3 mm ahead of the notch, under similar (low mean stress) conditions, prior to static loading.

Fatigue crack growth tests were carried out either at atmospheric pressure, or at better than 2.10^{-7} mbar total pressure. Test frequencies ranged from 60 to 0.1 Hz. In most tests a mean stress, R = 0.5 where $R = K_{min}/K_{max}$ (and K is the linear elastic stress intensity factor) was employed.

Crack growth was measured by the DC potential drop technique. To avoid the problems inherent to this technique under vacuum conditions (Bowen (6)) all tests were performed under increasing stress intensity conditions. Under static loading, K has been used successfully to characterise the rate of crack growth with time da/dt (Hippsley (7), Shin and McMahon (8)), and this parameter is used in the present study. Under cyclic loading, the alternating fatigue stress intensity range, ΔK (where $\Delta K = K_{max} - K_{min}$) is used to characterise the increment of crack growth per cycle, da/dN. Most tests were completed within eight hours and therefore large changes in matrix strength due to tempering were avoided, see table 2.

After testing at 500 °C, testpieces were broken open at low temperatures (typically -150 °C) to expose the high temperature crack surfaces for fractographic analysis. High resolution fractography was carried out, using an Hitachi S-570 scanning electron microscope. Attention was directed primarily towards examining surfaces produced in vacuum tests. For crack growth under static

loading, fractographic features were compared at equivalent values of stress intensity K, for the range of heat treatments employed. For crack growth under cyclic loading, attention was focused on comparisons of fractographic features for the condition directly water quenched from 1300 °C, at positions of equivalent fatigue stress intensity ΔK, and at frequencies of 10 and 0.1 Hz.

In two additional testpieces, representing the extremes of quench conditions, and testing under intermediate vacuum conditions ($\leq 1.10^{-3}$ mbar), static tests were interrupted at a K of 52 MPa $\sqrt{m}$ by unloading and cooling rapidly to room temperature. Specimens suitable for Auger electron spectroscopy could then be machined from each testpiece to include the high temperature crack tip. When broken open in the fracture stage of a Vacuum Generators MA500 Auger system, the crack tip surface chemistry and the interfacial chemistry of the embrittled grain boundaries immediately in front of the crack tip, could be analysed and compared with those embrittled boundaries remote from the crack tip region. Further details of this procedure are given elsewhere (1), (3). All Auger electron spectra were obtained in the direct pulse-counting mode (N(E) versus E) using a beam current of 20 nA at an accelerating voltage of 10 kV. These spectra were then differentiated numerically to provide the more familiar double peaks (dN(E)/d(E) versus E) which are used to quantify the concentrations of elements detected.

RESULTS

Crack Growth under Monotonic Loading

The dependence of crack growth rate, da/dt, on the stress intensity, K, is shown in figure 3 for the full range of quenched conditions. These tests were performed in vacua of approximately 1.10^{-3} mbar total pressure. There is a linear relationship between the stress intensity, K, and the logarithm of the crack growth rate, log (da/dt). The results also give a linear relationship between the logarithm of the stress intensity, log K, and the logarithm of the crack growth rate, log(da/dt). Most importantly, from figure 3 it can be seen that as the final austenitising temperature prior to quenching decreases, then the crack growth resistance increases. Fractographic observations indicate that the fracture mechanism is 100% intergranular in all cases. However, for all quenched conditions, the mechanism of intergranular fracture changes as a function of K. Consider the testpiece quenched directly from 1300 °C. At values of K less than 55 MPa $\sqrt{m}$ the intergranular separation is smooth, although some ridges (indicative of stepwise growth) are observed normal to the crack growth direction, figure 4(a), while at values of K greater than 55 MPa $\sqrt{m}$, intergranular microvoid coalescence is seen, figure 4(b). Mi-

crovoids of two distinct scales are observed at higher magnification (5). It is of interest to note that this transition occurs for all quenched conditions over a comparatively narrow range of K from 45 to 55 MPa $\sqrt{m}$, but over a wide range of crack growth rates, da/dt, from 7.10^{-2} to 1.10^{-4} mms^{-1}. If the extremes of quenched conditions are compared at the same crack growth rate of 3.10^{-4} mms^{-1}, the difference in the mechanism of intergranular fracture is marked - compare figure 5(a) and (b).

Examples of the Auger electron spectra obtained from testpieces interrupted during high temperature cracking (and representing the extremes of quenched conditions) are shown in figure 6(a) and (b). The interfacial composition of grain boundaries distant from the highly stressed crack tip region in both specimens comprised iron, oxygen, carbon and segregated phosphorus, figure 6(a). The high temperature crack surfaces were heavily contaminated with carbon, and this element was therefore used to locate those grain boundaries close to the crack tips. In both quenched conditions, significant increases in sulphur concentrations were measured in these crack tip regions, figure 6(b). Intriguingly, the average surface concentration of sulphur was similar in both quenched conditions at approximately 3.5 atomic %.

For the extremes of quenched conditions tested in air, there is a much reduced effect of the final austenitising temperature prior to quenching on the crack growth rate, da/dt, versus stress intensity, K, dependence - see figure 7.

Strong environmental effects are observed on the crack growth rate versus stress intensity dependence. In figure 8, this is shown for the condition quenched from 1300 °C.

Crack Growth under Cyclic Loading

For the condition directly quenched from 1300 °C, the crack growth resistance curves obtained in vacuum (better than 2.10^{-7} mbar) and in air are shown in figures 9 and 10 respectively. Note in figures 9 and 10 that the fatigue stress intensity, ΔK, has been plotted versus the logarithm of the crack increment per cycle, log(da/dN). Strong effects of frequency on da/dN are observed in both air and vacuum. For the highest test frequencies used (and low mean stress, R = 0.1), no intergranular facets are seen on the fracture surfaces, and crack advance occurs by "striation" growth. At all other test frequencies (and high mean stress, R = 0.5) the fracture surfaces are almost entirely intergranular, and are generally indistinguishable from those produced under static conditions. Under vacuum conditions, however, there is an effect of frequency on the mechanism of intergranular frac-

ture - see figures 11 and 12. At the lowest test frequency employed, 0.1 Hz, the facets produced are smoother and exhibit less microductility than those produced at 10 Hz for equivalent fatigue stress intensity conditions. It should be noted that the crack growth rate with respect to time, da/dt, is closely similar at both these frequencies, and in fact at the highest ΔK, the crack growth with time at 0.1 Hz is faster than at 10 Hz - see figure 9.

DISCUSSION

Crack Growth under Monotonic Loading

In figure 3, it is observed that the crack growth resistance curves in vacuum, are strongly dependent on the final austenitising temperature prior to quenching. Crack growth resistance increases as this final austenitising temperature decreases. Since phosphorus concentrates more strongly at grain boundaries as the final austenitising temperature is decreased, then phosphorus is not the primary embrittling species responsible for this form of cracking. However, the observations are consistent with sulphur being the most potent embrittling agent, and, in particular, the results indicate that the amount of sulphur present in solid solution is critical - see table 3. The dynamic segregation of sulphur to stressed crack-tip regions is directly confirmed by the Auger electron spectra shown in figure 6. Scanning Auger Microscopy studies have revealed the same concentration of sulphur ahead of crack tips in specimens from the extremes of the quenched conditions, at equivalent stress intensity, K. Therefore, for a given stress intensity, K, it appears that there is a critical invariant concentration (or coverage) of sulphur required to cause intergranular fracture, i.e. at a stress intensity of 52 MPa $\sqrt{m}$, a concentration of 3.5 atomic % sulphur is required (see also references 1 and 5).

The intergranular fracture mechanism changes from LDIGF to intergranular microvoid coalescence (IMVC) as a function of stress intensity, figure 4. The IMVC mechanism dominates only at high stress intensities, greater than approximately 55 MPa $\sqrt{m}$. The transition is envisaged to occur as a result of a competition between the smooth, featureless intergranular fracture, controlled by a critical coverage of sulphur, and the intergranular microvoid coalescence fracture controlled by plasticity-induced void nucleation and growth (around sulphides and carbides).

For static tests performed in air the crack growth rates are much higher than those in vacuum and there is a reduced dependence of the crack growth rates on the final austenitising temperature prior to quenching - see figures 7 and 8. From a practical viewpoint, the growth of surface cracks will therefore be much more deleterious to structural integrity than the growth of buried cracks. It is clear that there is some active embrittling species

(possibly oxygen) present in the air environment which dramatically encourages the crack growth process. In air, these forms of cracking phenomenon may then be best considered as a form of stress corosion cracking. Further work is proceeding to investigate these effects more fully.

Crack Growth under Cyclic Loading

Pronounced effects of frequency are observed on the crack increment per cycle, da/dN, in both air and vacuum. The crack increment per cycle increases as the frequency decreases. At frequencies of 10, 1 and 0.1 Hz, at high mean stress, crack growth is 100% intergranular. The closely similar fracture morphology observed for both cyclic and monotonic loading (compare figures 11 and 4) suggests strongly that the static mechanism of crack growth dominates during fatigue loading. Therefore, it is of considerable interest to investigate whether the increases in crack increment per cycle, da/dN, produced as the frequency is reduced from 10 to 0.1 Hz, can be predicted from base line fatigue data at high frequency and low mean stress (and containing no intergranular facets) and the appropriate static resistance curve intergrated over one fatigue cycle. This is treated in detail elsewhere (Bowen et al. (9), but one set of predictions for growth in air is shown in figure 13. These predictions have been made by simply adding the base line fatigue data to the crack growth increment per cycle predicted from the static mechanism. The static component is calculated using a growth law of the form:

$$da/dt = CK^m \qquad (1)$$

where C and m are numerical constants. Integration over one fatigue cycle is made by substituting K in terms of ΔK (the resulting definite integral can be solved analytically for integer values of m). This approach can be seen in figure 13 to give excellent predictions of the enhancement of da/dN at lower frequencies for tests performed in air. Similar predictions can be made for tests performed in vacuum (9). The method of analysis appears to have useful potential for modeling fatigue creep interactions.

Careful examination of the fracture surfaces produced in vacuum after testing at the frequencies of 0.1 and 10 Hz, tends to support the approach suggested for the modelling of the fatigue crack growth. The intergranular facets produced by testing at 0.1 Hz are smooth and do not show evidence of micro-ductility (figure 11). Those produced by testing at 10 Hz under equivalent fatigue stress intensities do show significant evidence of micro-ductility (figure 12). As for growth under constant load, there is presumably a competition between the amount of sulphur which segregates ahead of a crack tip in a given period of time (this promoting LDIGF) and now the "mechanical" increment of fatigue crack growth

"forced" by the applied stress intensity range. It is intriguing to note that, although the contribution of LDIGF to the crack growth increment per cycle is increased at the lower frequency (0.1 Hz), a simple interpretation in terms of greater time for sulphur diffusion cannot be sustained because the crack growth rates with respect to time, da/dt, obtained at 0.1 Hz are equal to, or greater than, those obtained at 10 Hz - see figure 9.

Therefore, the rapidly alternating stress cycle (at 10 Hz) either retards the mechanism of sulphur segregation in some manner, or promotes the nucleation and growth of microvoids. Further work is continuing in this area.

CONCLUSIONS

1. Coarse-grained martensitic 2¼Cr-1Mo, suffers from subcritical intergranular crack growth in air and in vacuum, when tested at 500 °C. Crack growth resistance is dramatically reduced in air.

2. In vacuum, sulphur is the primary embrittling species responsible for the observed low ductility intergranular fracture. Sulphur is found to segregate dynamically to crack tip regions, and it appears that a critical concentration of sulphur is required to cause low ductility intergranular fracture. In particular, decreasing the amount of sulphur remaining in solid solution promotes crack growth resistance.

3. In vacuum, the mechanism of intergranular fracture changes at high stress intensities from low ductility intergranular fracture to intergranular microvoid coalescence.

4. In air, the crack growth resistance is considerably less dependent on the amount of sulphur remaining in solid solution. An environmental interaction strongly encourages the crack growth process. Therefore, in air, such high temperature crack growth may be considered as a form of stress corrosion cracking.

5. Both mechanisms of subcritical intergranular cracking can occur during fatigue loading in air and in vacuum. Large increases in crack increment per cycle, da/dN, are observed as the frequency is reduced, both in air and in vacuum. These can be accurately predicted from base line fatigue data and the appropriate static growth resistance curve integrated over one fatigue cycle.

REFERENCES

(1) Hippsley, C.A., Rauh, H. and Bullough, R., Acta metall., Vol. 32, 1984, pp. 1381-1394.

(2) Shin, J. and McMahon, C.J., Met. Sci., Vol. 18, 1984, pp. 403-410.

(3) Bowen, P., Hippsley, C.A. and Knott, J.F., Acta metall., Vol. 32, 1984, pp. 637-647.

(4) Turdogan, E.T., Ignatowicz, S. and Pearson, J., J.I.S.I., Vol. 80, 1955, pp. 349-354.

(5) Hippsley, C.A. and Bowen, P., submitted to Acta metall.

(6) Bowen, P., Ph. D. Thesis, University of Cambridge, November 1984.

(7) Hippsley, C.A., Met. Sci., Vol. 17, 1983, pp. 277-288.

(8) Shin, J. and McMahon, C.J., Acta metall., 1984, Vol. 32, pp. 1535-1552.

(9) Bowen, P., Hippsley, C.A. and Knott, J.F., submitted to Fat. Eng. Mat. and Structures.

ACKOWLEDGEMENTS

One of the authors (PB) was supported in the course of this work by a SERC postdoctoral award, and by a Goldsmiths' Junior Research Fellowship at Churchill College, Cambridge. Further support from the Department of Trade and Industry (as part of the COST 505 exercise) is also gratefully ackowledged. Thanks are also due to Professor D. Hull for the provision of research facilities.

TABLE 1 - Composition of 2¼Cr-1Mo plate, wt.%

	Cr	Mo	Mn	Si	Ni	C	P	S
Commercial purity	2.12	0.95	0.53	0.17	0.20	0.13	0.015	0.021

TABLE 2 - Hardness values and 0.2% Proof Stress values at room temperature

Condition	$V_H(30)$ (as quenched)	$V_H(30)$ (after 8h at 500°C)	0.2% Proof Stress (MPa) (as quenched)
1300,WQ	406 ± 9	366 ± 4	1060
1300-900,WQ	409 ± 7	368 ± 2	1060

TABLE 3 - Equilibrium concentration (Co) of sulphur in iron containing 0.53 Mn (wt.%)

	Temperature (°C)				
	1300	1200	1100	1000	900
Co (ppm)	31.0	12.8	4.7	1.4	0.4

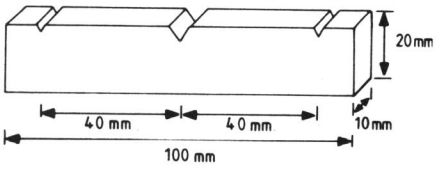

Fig. 1 Notched bend testpiece

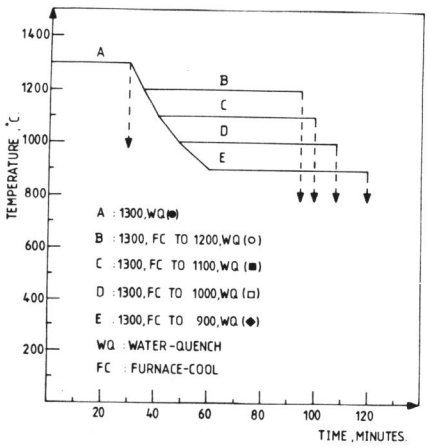

Fig. 2 Heat-treatment schedules

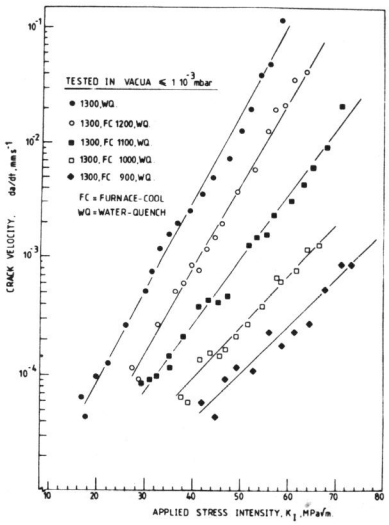

Fig. 3 Crack growth resistance curves in vacuum ($\lesssim 1.10^{-3}$ mbar)

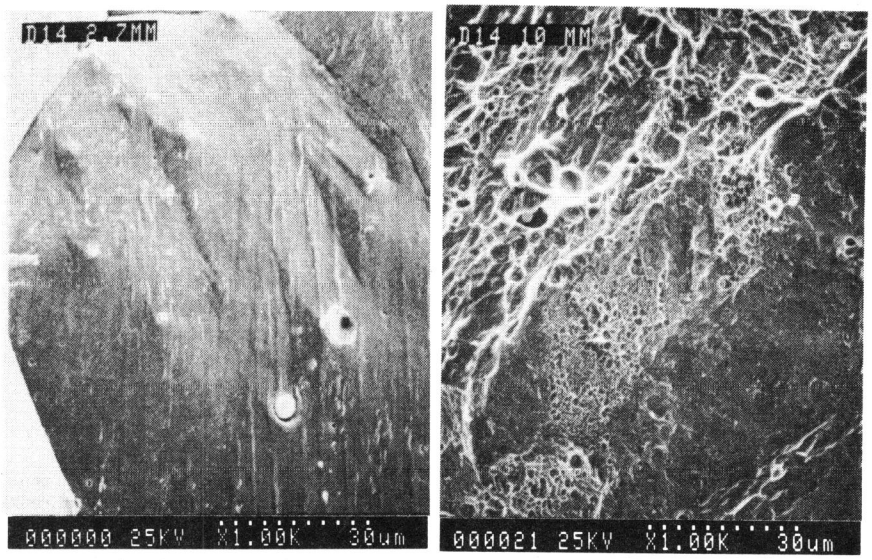

(a) (b)

Fig. 4 In vacuum ($\lesssim 1.10^{-3}$ mbar), 1300 WQ condition, (a) K= 40 MPa$\sqrt{m}$ (b) K=60 MPa$\sqrt{m}$.

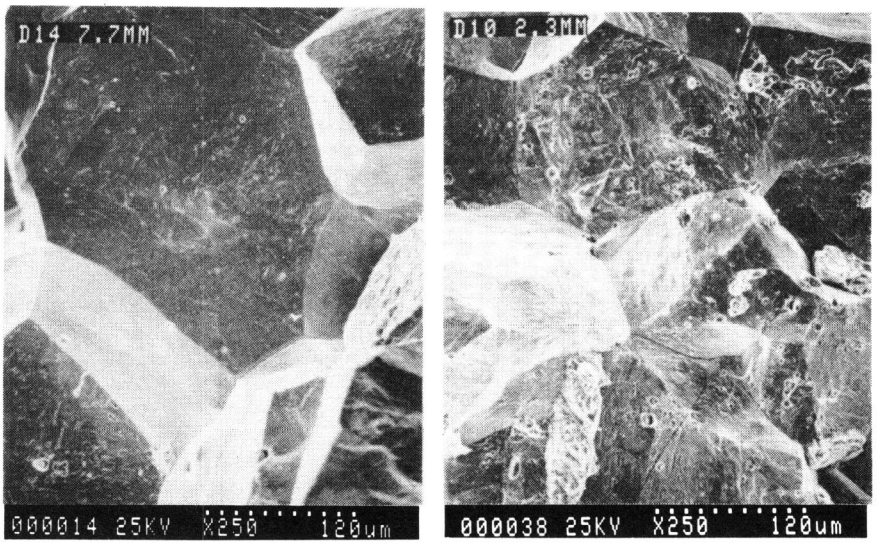

(a) (b)

Fig. 5 In vacuum ($\lesssim 1.10^{-3}$mbar), da/dt=3.10^{-4} mms^{-1} (a) 1300 WQ condition (b) 1300-900 WQ condition.

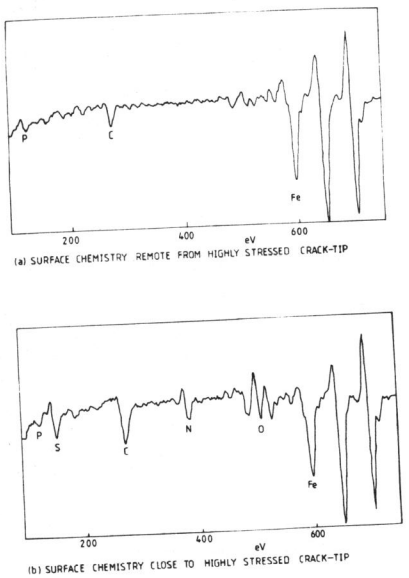

Fig. 6 Auger electron spectra (dN(E)/d(E) versus E)

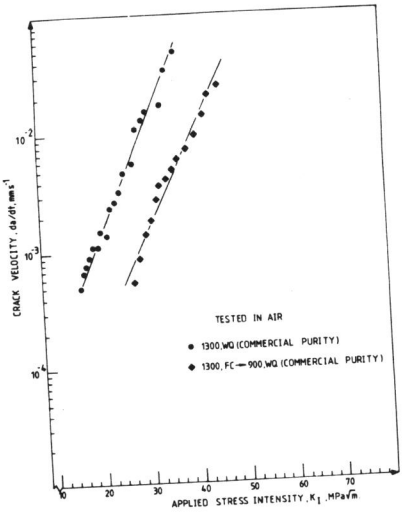

Fig. 7 Crack growth resistance curves in air

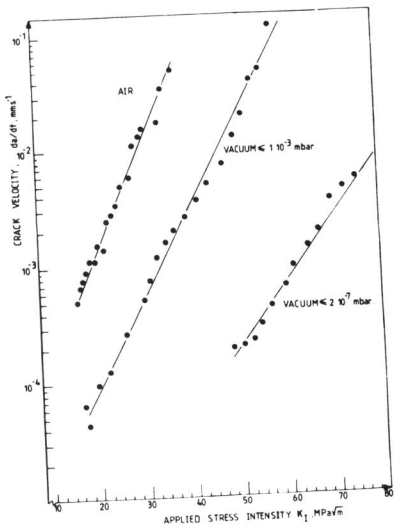

Fig. 8 Effect of environment on 1300 WQ condition

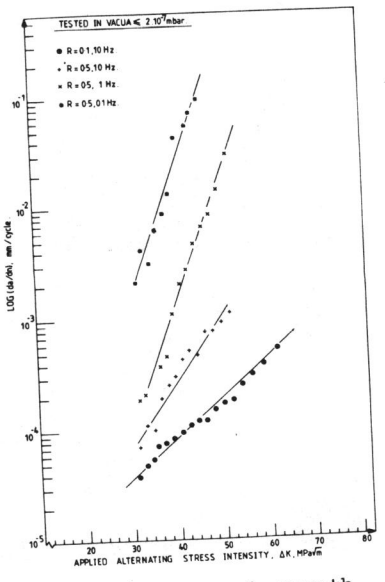

Fig. 9 Fatigue crack growth resistance curves in vacuum

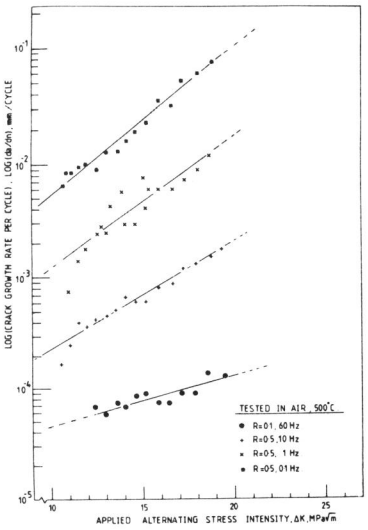

Fig. 10 Fatigue crack growth resistance curves in air

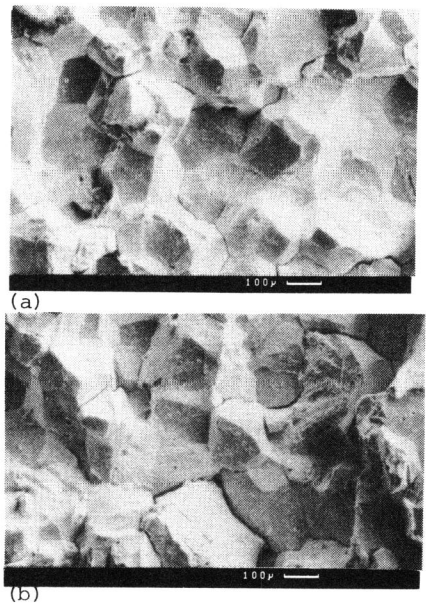

Fig. 11 In vacuum, ν=0.1Hz (a) $\Delta K = 33 MPa\sqrt{m}$ (b) $\Delta K = 52 MPa\sqrt{m}$.

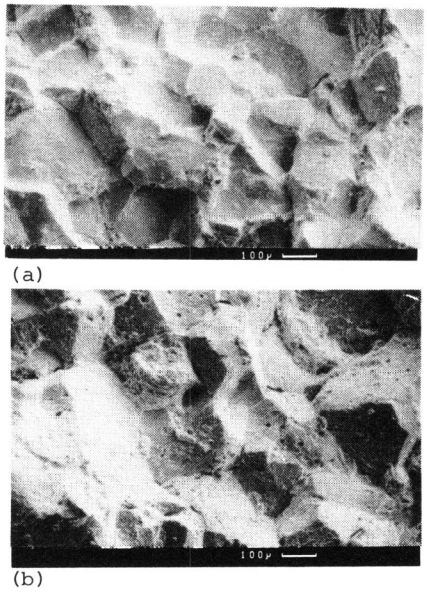

Fig. 12 In vacuum, ν=10Hz (a) $\Delta K = 33 MPa\sqrt{m}$ (b) $\Delta K = 52 MPa\sqrt{m}$.

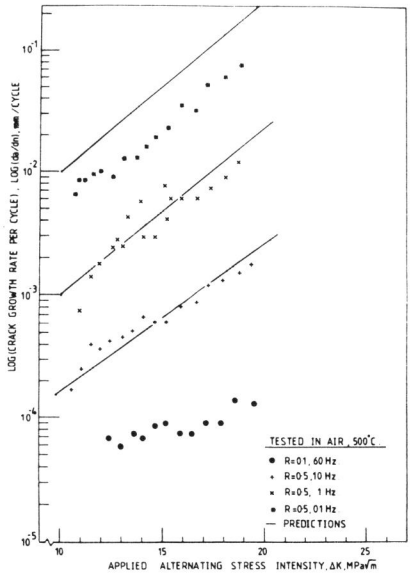

Fig. 13 Predictions of crack growth resistance in air